2025 International Conference on
Unmanned Aircraft Systems (ICUAS)
May 14-17, 2025. North Carolina, USA

Dynamics and Control of a Hexacopter Propelled by Three Seesaws

Dolev Yecheskel[1] and Shai Arogeti[2]

***Abstract*— Standard drones propelled by four rotors are under-actuated systems. They use four control inputs to control four degrees of freedom independently. Hexacopters are driven by two more propellers, but since the direction of the total thrust remains normal to the drone's body, still only four degrees of freedom can be controlled independently. In this study, we describe a new hexacopter type consisting of three seesaws. Each seesaw is driven by two propellers, allowing rotation of the seesaw relative to the drone's body. Then, we develop the drone's unique control system and demonstrate its ability to maneuver with six controlled degrees of freedom while propelled by six motors only.**

***Index Terms*—Hexacopter, Fully-actuated drones, Drones with seesaws.**

I. Introduction

Drones have many advantages as robotic platforms. These advantages are mainly based on the possibility of vertical take-off and landing and the drone's hovering capability. Current applications include aerial photography and aerial transport of small cargo. These applications were tailored to the drone's unique capabilities, but, also to its weaknesses. Standard drones are under-actuated systems, which means it is impossible to control all of their six degrees of freedom independently. Generally, only the three position coordinates and the heading are directly controlled, while the orientation (including the pitch and roll) is derived from the commanded motion (e.g., they are utilized as virtual control signals of the position controller in a hierarchical control structure). For applications that require a specific angular state, mechanical auxiliary devices, such as active gimbals, are attached to the drone. These add weight and complexity.

In recent years, drones with an unusual structure have been suggested. The main goal of these new structures is to expand the drone's motion abilities and enable new applications; for example, to allow physical interaction of the drone with other ground objects where it applies a desired force [1], [2], [3]. The new structures usually belong to one of two configurations: a fixed tilting configuration and an active tilting configuration. In an active tilting configuration, additional actuators must be added to the structure to allow active tilting of the thrust forces [4], [5], [6]. In the fixed tilting configuration, the thrust directions relative to the aircraft body are pre-selected to allow movement in any desired direction [7], [8] [9]. In these cases, no additional actuators are required other than those used to generate thrust, but due to the loss of energy efficiency, the challenge is often in finding the optimal static thrust configuration [10], [11]. It is also known that tilted propellers create a stabilizing effect and allow for better resistance to the influence of disturbances [12], [13]. Full actuation can also result from a physical connection of several drones [14].

In this study, we suggest an innovative structure based on three seesaws. The idea is to use free-rotating seesaws to tilt thrust forces actively. In [15], we suggested a hexacopter with a single seesaw. Four propellers were attached to the main body (performing as a standard quadcopter), while the other two were attached to the seesaw. This configuration provided an additional degree of freedom for the main body that can be controlled independently (i.e., pitch or roll). In [16], we suggested an octocopter with eight propellers and four seesaws. That configuration was, in fact, over-actuated at the cost of two extra unnecessary propellers. Here, we suggest a balanced structure with six propellers. It utilizes six motors to control independently six (body's) degrees of freedom. There are no other actuators carried by the drone that do not contribute to the lift (such as [17]). Another advantage over other thrust-tilting mechanisms (e.g., [18]) is that the suggested seesaw structure does not pose any mechanical limit on the tilting angle.

The rest of the paper is organized as follows. Section II describes the drone, its structure, and its motion principles. The mathematical model, including the kinematics, dynamics, and actuation, is developed in section III. In section IV, we develop a control system for the drone and demonstrate its capabilities numerically. Then, section V concludes the paper.

II. Three-Seesaw Hexacopter

This section includes a description of the drone's unique structure and motion.

A. Structure

The structure of the three-seesaw hexacopter is presented in Fig. 1. The main body functions as a hub to which three seesaws are attached. The seesaws are evenly distributed. Hence, the angle between two adjacent seesaws is $\frac{\pi}{3}\,[\mathrm{rad}]$. The seesaws are supported in the main body by bearings, which allow them to rotate freely. The angle at each seesaw (with respect to the body) is measured by an incremental encoder installed at the seesaw hinge. Each seesaw is powered by two propellers, resulting in a total of six propellers controlling the drone.

B. Motion

To describe the drone's motion, five coordinate systems are defined. The inertial coordinate system is attached to

[1]Dolev Yecheskel completed his Master's degree at the department of mechanical engineering, Ben-Gurion University of the Negev, Israel

[2]Shai Arogeti is with the Department of Mechanical Engineering, Ben-Gurion University of the Negev, Israel, (e-mail: arogeti@bgu.ac.il).

2025 International Conference on Unmanned Aircraft Systems (ICUAS) | 979-8-3315-1328-3/25/$31.00 ©2025 IEEE | DOI: 10.1109/ICUAS65942.2025.11007797

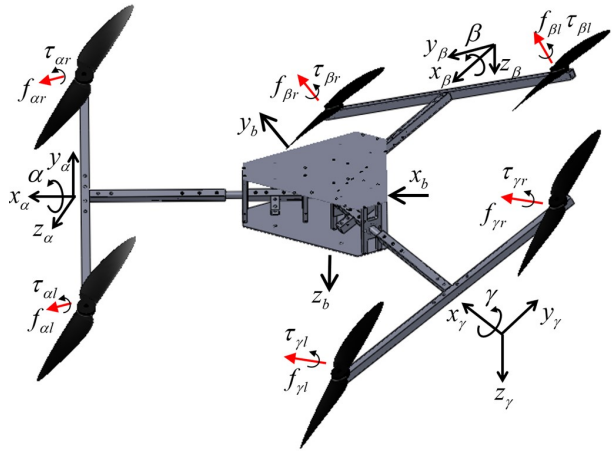

Fig. 1. The structure of the three-seesaw Hexacopter

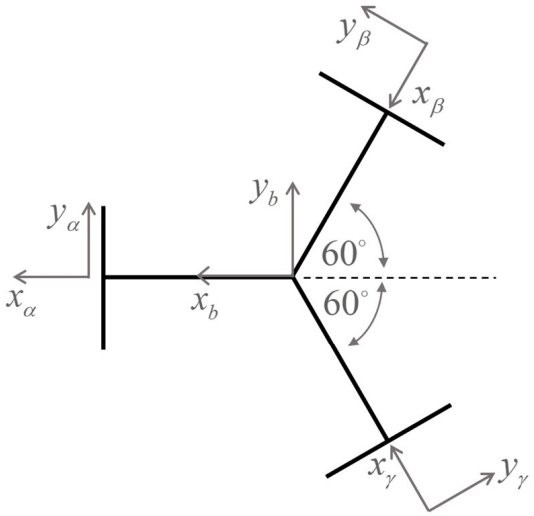

Fig. 2. Local coordinate systems - top view

the ground; it is a standard NED system with the three-unit vectors $\hat{e} = [\hat{x}_e, \hat{y}_e, \hat{z}_e]^T$ (where, $\hat{z}_e$ points down). The body coordinate system is attached to the body and represented by $\hat{b} = [\hat{x}_b, \hat{y}_b, \hat{z}_b]^T$. The unit vector $\hat{x}_b$ represents the drone's longitudinal axis, while $\hat{y}_b$ is the lateral direction. The position of the body in the inertial coordinate system is defined by the three coordinates (x, y, z). To describe the body's orientation, we will use the standard set of three Euler angles (ϕ, θ, ψ). Here, ϕ is the roll angle (rotation about $\hat{x}_b$), θ is the pitch angle (rotation with respect to $\hat{y}_b$), and ψ is the yaw angle (around $\hat{z}_b$). In total, the body is represented by six degrees of freedom, three for position and three for orientation. Additionally, there are three internal degrees of freedom to represent the seesaw's state with respect to the body. The angle of the front seesaw is represented by α, the angle of the rear right seesaw is β and for the rear left seesaw, the angle is γ. Accordingly, three seesaws' coordinate systems are defined, notated by $\hat{\alpha} = [\hat{x}_\alpha, \hat{y}_\alpha, \hat{z}_\alpha]^T$, $\hat{\beta} = [\hat{x}_\beta, \hat{y}_\beta, \hat{z}_\beta]^T$ and $\hat{\gamma} = [\hat{x}_\gamma, \hat{y}_\gamma, \hat{z}_\gamma]^T$; these coordinate systems are attached to the seesaws. In total, the motion of the drone is described by nine degrees of freedom, which includes the six body degrees of freedom and the three seesaw angles (α, β, γ). The control goal is to fully (or independently) control the motion of the body; the motion of the seesaws is considered internal and utilized to maneuver the body. The following notation will be used in the development of the drone's dynamical model; $\hat{e}_1 = [1, 0, 0]^T$, $\hat{e}_2 = [0, 1, 0]^T$ and $\hat{e}_3 = [0, 0, 1]^T$

III. Mathematical Model

Here, we develop the dynamical model required for the drone's control system design. In the first stage, the kinematical relations are formulated.

A. Kinematics

The angular state of the body is represented by the rotation matrix ${}^eR_b = {}^eR_{bz}{}^eR_{by}{}^eR_{bx}$. It results from a series of three rotations (where c· represents $\cos(\cdot)$ and s· is $\sin(\cdot)$),

$$
\begin{aligned}
{}^eR_{bx} &= \begin{bmatrix} 1 & 0 & 0 \\ 0 & \mathrm{c}\phi & -\mathrm{s}\phi \\ 0 & \mathrm{s}\phi & \mathrm{c}\phi \end{bmatrix}, {}^eR_{by} = \begin{bmatrix} \mathrm{c}\theta & 0 & \mathrm{s}\theta \\ 0 & 1 & 0 \\ -\mathrm{s}\theta & 0 & \mathrm{c}\theta \end{bmatrix}, \\
{}^eR_{bz} &= \begin{bmatrix} \mathrm{c}\psi & -\mathrm{s}\psi & 0 \\ \mathrm{s}\psi & \mathrm{c}\psi & 0 \\ 0 & 0 & 1 \end{bmatrix}.
\end{aligned} \tag{1}
$$

The obtained rotation matrix is,

$$
{}^eR_b = \begin{bmatrix} \mathrm{c}\psi\mathrm{c}\theta & \mathrm{c}\psi\mathrm{s}\theta\mathrm{s}\phi - \mathrm{s}\psi\mathrm{c}\phi & \mathrm{c}\psi\mathrm{s}\theta\mathrm{c}\phi + \mathrm{s}\psi\mathrm{s}\phi \\ \mathrm{s}\psi\mathrm{c}\theta & \mathrm{s}\psi\mathrm{s}\theta\mathrm{s}\phi + \mathrm{c}\psi\mathrm{c}\phi & \mathrm{s}\psi\mathrm{s}\theta\mathrm{c}\phi - \mathrm{c}\psi\mathrm{s}\phi \\ -\mathrm{s}\theta & \mathrm{c}\theta\mathrm{s}\phi & \mathrm{c}\theta\mathrm{c}\phi \end{bmatrix} \tag{2}
$$

and ${}^bR_e = [{}^eR_b]^T$, where the notation means $\hat{b} = {}^bR_e\hat{e}$.

Figure 2 depicts a top view of the drone with all local coordinate systems. Based on this description, three more rotation matrices are calculated to describe the influence of the seesaws' rotation. To transform from body coordinates to the front seesaw coordinates we use $\hat{\alpha} = {}^\alpha R_b\hat{b}$, where,

$$
{}^\alpha R_b = \begin{bmatrix} 1 & 0 & 0 \\ 0 & \mathrm{c}\alpha & \mathrm{s}\alpha \\ 0 & -\mathrm{s}\alpha & \mathrm{c}\alpha \end{bmatrix}. \tag{3}
$$

Accordingly, we have, $\hat{\beta} = {}^\beta R_b\hat{b}$ and $\hat{\gamma} = {}^\gamma R_b\hat{b}$, with,

$$
\begin{aligned}
{}^\beta R_b &= \begin{bmatrix} \mathrm{c}\frac{\pi}{3} & -\mathrm{s}\frac{\pi}{3} & 0 \\ \mathrm{s}\frac{\pi}{3}\mathrm{c}\beta & \mathrm{c}\frac{\pi}{3}\mathrm{c}\beta & \mathrm{s}\beta \\ -\mathrm{s}\frac{\pi}{3}\mathrm{s}\beta & -\mathrm{c}\frac{\pi}{3}\mathrm{s}\beta & \mathrm{c}\beta \end{bmatrix}, \\
{}^\gamma R_b &= \begin{bmatrix} \mathrm{c}\frac{\pi}{3} & \mathrm{s}\frac{\pi}{3} & 0 \\ -\mathrm{s}\frac{\pi}{3}\mathrm{c}\gamma & \mathrm{c}\frac{\pi}{3}\mathrm{c}\gamma & \mathrm{s}\gamma \\ \mathrm{s}\frac{\pi}{3}\mathrm{s}\gamma & -\mathrm{c}\frac{\pi}{3}\mathrm{s}\gamma & \mathrm{c}\gamma \end{bmatrix},
\end{aligned} \tag{4}
$$

for the two rear seesaws.

The dynamical model is derived in the next subsection from Euler–Lagrange equations, which requires formulating an expression for the kinetic energy of all bodies. It is easier to represent the kinetic energy in the local coordinate system, where the moment of inertia is constant. For that, the

following Jacobians are derived; they represent the angular velocity (due to $\dot{\phi}$, $\dot{\theta}$, $\dot{\psi}$ and the rotation of the seesaws) in local coordinates. We begin with the angular velocity of the body Ω_b, and represent all individual Euler-angles rates in the body frame. We then sum up their contribution to the body's angular velocity. The result is,

$$\begin{aligned}\Omega_b &= \begin{bmatrix} p_b \\ q_b \\ r_b \end{bmatrix} = \dot{\phi}\hat{e}_1 + {}^{b}R_{ex}\dot{\theta}\hat{e}_2 + {}^{b}R_{ex}{}^{b}R_{ey}\dot{\psi}\hat{e}_3 \\ &= \begin{bmatrix} 1 & 0 & -\mathrm{s}\theta \\ 0 & \mathrm{c}\phi & \mathrm{s}\phi\mathrm{c}\theta \\ 0 & -\mathrm{s}\phi & \mathrm{c}\phi\mathrm{c}\theta \end{bmatrix} \begin{bmatrix} \dot{\phi} \\ \dot{\theta} \\ \dot{\psi} \end{bmatrix} = J_{\Omega b} \begin{bmatrix} \dot{\phi} \\ \dot{\theta} \\ \dot{\psi} \end{bmatrix}.\end{aligned} \tag{5}$$

Following the same procedure, we have for the front seesaw,

$$\begin{aligned}\Omega_\alpha &= \begin{bmatrix} p_\alpha \\ q_\alpha \\ r_\alpha \end{bmatrix} \\ &= \dot{\alpha}\hat{e}_1 + \dot{\phi}\hat{e}_1 + {}^{\alpha}R_b{}^{b}R_{ex}\dot{\theta}\hat{e}_2 + {}^{\alpha}R_b{}^{b}R_{ex}{}^{b}R_{ey}\dot{\psi}\hat{e}_3 \\ &= \begin{bmatrix} 1 & 1 & 0 & -\mathrm{s}\theta \\ 0 & 0 & \mathrm{c}(\alpha+\phi) & \mathrm{s}(\alpha+\phi)\mathrm{c}\theta \\ 0 & 0 & -\mathrm{s}(\alpha+\phi) & \mathrm{c}(\alpha+\phi)\mathrm{c}\theta \end{bmatrix} \begin{bmatrix} \dot{\alpha} \\ \dot{\phi} \\ \dot{\theta} \\ \dot{\psi} \end{bmatrix} = J_{\Omega\alpha} \begin{bmatrix} \dot{\alpha} \\ \dot{\phi} \\ \dot{\theta} \\ \dot{\psi} \end{bmatrix},\end{aligned} \tag{6}$$

where this Jacobian is also influenced by the seesaw angular state. Accordingly for the two rear seesaws, the resulting Jacobians would be,

$$\begin{aligned}\Omega_\beta &= \begin{bmatrix} p_\beta \\ q_\beta \\ r_\beta \end{bmatrix} = J_{\Omega\beta} \begin{bmatrix} \dot{\beta} \\ \dot{\phi} \\ \dot{\theta} \\ \dot{\psi} \end{bmatrix} \\ &= \dot{\beta}\hat{e}_1 + {}^{\beta}R_b\dot{\phi}\hat{e}_1 + {}^{\beta}R_b{}^{b}R_{ex}\dot{\theta}\hat{e}_2 + {}^{\beta}R_b{}^{b}R_{ex}{}^{b}R_{ey}\dot{\psi}\hat{e}_3 \\ &= \begin{bmatrix} 1 & \mathrm{c}\frac{\pi}{3} & -\mathrm{s}\frac{\pi}{3}\mathrm{c}\phi & -\mathrm{c}\frac{\pi}{3}\mathrm{s}\theta - \mathrm{s}\frac{\pi}{3}\mathrm{s}\phi\mathrm{c}\theta \\ 0 & \mathrm{s}\frac{\pi}{3}\mathrm{c}\beta & \begin{pmatrix}\mathrm{c}\frac{\pi}{3}\mathrm{c}\beta\mathrm{c}\phi \\ -\mathrm{s}\beta\mathrm{s}\phi\end{pmatrix} & \begin{pmatrix}-\mathrm{s}\frac{\pi}{3}\mathrm{c}\beta\mathrm{s}\theta \\ +\mathrm{c}\frac{\pi}{3}\mathrm{c}\beta\mathrm{s}\phi\mathrm{c}\theta \\ +\mathrm{s}\beta\mathrm{c}\phi\mathrm{c}\theta\end{pmatrix} \\ 0 & -\mathrm{s}\frac{\pi}{3}\mathrm{s}\beta & \begin{pmatrix}-\mathrm{c}\frac{\pi}{3}\mathrm{s}\beta\mathrm{c}\phi \\ -\mathrm{c}\beta\mathrm{s}\phi\end{pmatrix} & \begin{pmatrix}\mathrm{s}\frac{\pi}{3}\mathrm{s}\beta\mathrm{s}\theta \\ -\mathrm{c}\frac{\pi}{3}\mathrm{s}\beta\mathrm{s}\phi\mathrm{c}\theta \\ +\mathrm{c}\beta\mathrm{c}\phi\mathrm{c}\theta\end{pmatrix} \end{bmatrix} \begin{bmatrix} \dot{\beta} \\ \dot{\phi} \\ \dot{\theta} \\ \dot{\psi} \end{bmatrix}\end{aligned} \tag{7}$$

and

$$\begin{aligned}\Omega_\gamma &= \begin{bmatrix} p_\gamma \\ q_\gamma \\ r_\gamma \end{bmatrix} = J_{\Omega\gamma} \begin{bmatrix} \dot{\gamma} \\ \dot{\phi} \\ \dot{\theta} \\ \dot{\psi} \end{bmatrix} \\ &= \dot{\gamma}\hat{e}_1 + {}^{\gamma}R_b\dot{\phi}\hat{e}_1 + {}^{\gamma}R_b{}^{b}R_{ex}\dot{\theta}\hat{e}_2 + {}^{\gamma}R_b{}^{b}R_{ex}{}^{b}R_{ey}\dot{\psi}\hat{e}_3 \\ &= \begin{bmatrix} 1 & \mathrm{c}\frac{\pi}{3} & \mathrm{s}\frac{\pi}{3}\mathrm{c}\phi & -\mathrm{c}\frac{\pi}{3}\mathrm{s}\theta + \mathrm{s}\frac{\pi}{3}\mathrm{s}\phi\mathrm{c}\theta \\ 0 & -\mathrm{s}\frac{\pi}{3}\mathrm{c}\gamma & \begin{pmatrix}\mathrm{c}\frac{\pi}{3}\mathrm{c}\gamma\mathrm{c}\phi \\ -\mathrm{s}\gamma\mathrm{s}\phi\end{pmatrix} & \begin{pmatrix}\mathrm{s}\frac{\pi}{3}\mathrm{c}\gamma\mathrm{s}\theta \\ +\mathrm{c}\frac{\pi}{3}\mathrm{c}\gamma\mathrm{s}\phi\mathrm{c}\theta \\ +\mathrm{s}\gamma\mathrm{c}\phi\mathrm{c}\theta\end{pmatrix} \\ 0 & \mathrm{s}\frac{\pi}{3}\mathrm{s}\gamma & \begin{pmatrix}-\mathrm{c}\frac{\pi}{3}\mathrm{s}\gamma\mathrm{c}\phi \\ -\mathrm{c}\gamma\mathrm{s}\phi\end{pmatrix} & \begin{pmatrix}-\mathrm{s}\frac{\pi}{3}\mathrm{s}\gamma\mathrm{s}\theta \\ -\mathrm{c}\frac{\pi}{3}\mathrm{s}\gamma\mathrm{s}\phi\mathrm{c}\theta \\ +\mathrm{c}\gamma\mathrm{c}\phi\mathrm{c}\theta\end{pmatrix} \end{bmatrix} \begin{bmatrix} \dot{\gamma} \\ \dot{\phi} \\ \dot{\theta} \\ \dot{\psi} \end{bmatrix}\end{aligned} \tag{8}$$

The kinetic energy due to translation is assumed to be decoupled from the kinetic energy due to rotation (this assumption also holds for the potential energy). Therefore, we define two separate vectors of generalized coordinates, given by,

$$\xi = \begin{bmatrix} x \\ y \\ z \end{bmatrix} \Rightarrow \dot{\xi} \begin{bmatrix} \dot{x} \\ \dot{y} \\ \dot{z} \end{bmatrix}, \quad \sigma = \begin{bmatrix} \alpha \\ \beta \\ \gamma \\ \phi \\ \theta \\ \psi \end{bmatrix} \Rightarrow \dot{\sigma} = \begin{bmatrix} \dot{\alpha} \\ \dot{\beta} \\ \dot{\gamma} \\ \dot{\phi} \\ \dot{\theta} \\ \dot{\psi} \end{bmatrix}. \tag{9}$$

The position of the body is represented by $\xi \in \mathrm{R}^3$, while $\sigma \in \mathrm{R}^6$ represents the angular states. For a concise description of the angular kinetic energy, all Jacobian matrices are extended, such that they can operate directly on $\dot{\sigma}$. The extended body Jacobian is given by,

$$\begin{aligned}\Omega_b &= J_{\Omega b} \begin{bmatrix} \dot{\phi} \\ \dot{\theta} \\ \dot{\psi} \end{bmatrix} = \bar{J}_{\Omega b}\dot{\sigma} \quad \Rightarrow \\ \bar{J}_{\Omega b} &= \begin{bmatrix} 0 & 0 & 0 & 1 & 0 & -\mathrm{s}\theta \\ 0 & 0 & 0 & 0 & \mathrm{c}\phi & \mathrm{s}\phi\mathrm{c}\theta \\ 0 & 0 & 0 & 0 & -\mathrm{s}\phi & \mathrm{c}\phi\mathrm{c}\theta \end{bmatrix},\end{aligned} \tag{10}$$

and for the front seesaw, one has,

$$\begin{aligned}\Omega_\alpha &= J_{\Omega\alpha} \begin{bmatrix} \dot{\alpha} \\ \dot{\phi} \\ \dot{\theta} \\ \dot{\psi} \end{bmatrix} = \bar{J}_{\Omega\alpha}\dot{\sigma} \quad \Rightarrow \\ \bar{J}_{\Omega\alpha} &= \begin{bmatrix} 1 & 0 & 0 & 1 & 0 & -\mathrm{s}\theta \\ 0 & 0 & 0 & 0 & \mathrm{c}(\alpha+\phi) & \mathrm{s}(\alpha+\phi)\mathrm{c}\theta \\ 0 & 0 & 0 & 0 & -\mathrm{s}(\alpha+\phi) & \mathrm{c}(\alpha+\phi)\mathrm{c}\theta \end{bmatrix}.\end{aligned} \tag{11}$$

Following an identical procedure, the extended Jacobians of the two rear seesaws are $\bar{J}_{\Omega\beta}$ and $\bar{J}_{\Omega\gamma}$.

B. Dynamics

We assume that all involved bodies are symmetric and their inertia matrix given in the local coordinate frame is diagonal. The body inertia matrix is $I_b \in \mathrm{R}^3$, and the inertia matrices of the three seesaws are $I_\alpha \in \mathrm{R}^3$, $I_\beta \in \mathrm{R}^3$ and $I_\gamma \in \mathrm{R}^3$. The mass, including the body and seesaws, is m.

The total kinetic energy, expressed by local coordinates, is,

$$\begin{aligned}T = &\frac{1}{2}m\dot{\xi}^T\dot{\xi} + \frac{1}{2}\dot{\sigma}^T[\bar{J}_{\Omega b}]^T I_b \bar{J}_{\Omega b}\dot{\sigma} + \frac{1}{2}\dot{\sigma}^T[\bar{J}_{\Omega\alpha}]^T I_\alpha \bar{J}_{\Omega\alpha}\dot{\sigma} \\ &+ \frac{1}{2}\dot{\sigma}^T[\bar{J}_{\Omega\beta}]^T I_\beta \bar{J}_{\Omega\beta}\dot{\sigma} + \frac{1}{2}\dot{\sigma}^T[\bar{J}_{\Omega\gamma}]^T I_\gamma \bar{J}_{\Omega\gamma}\dot{\sigma}.\end{aligned} \tag{12}$$

The definition of extended Jacobian matrices allows us now to unify all the inertia terms related to the rotational motion,

$$T = \frac{1}{2}m\dot{\xi}^T\dot{\xi} + \frac{1}{2}\dot{\sigma}^T D\dot{\sigma} \tag{13}$$

where,

$$\begin{aligned}D = &[\bar{J}_{\Omega b}]^T I_b \bar{J}_{\Omega b} + [\bar{J}_{\Omega\alpha}]^T I_\alpha \bar{J}_{\Omega\alpha} \\ &+ [\bar{J}_{\Omega\beta}]^T I_\beta \bar{J}_{\Omega\beta} + [\bar{J}_{\Omega\gamma}]^T I_\gamma \bar{J}_{\Omega\gamma}\end{aligned} \tag{14}$$

is the unified inertia matrix. Adding also the potential energy due to gravity, the Lagrangian is expressed in the following way,

$$L = T - U = \frac{1}{2} m \dot{\xi}^T \dot{\xi} + \frac{1}{2} \dot{\sigma}^T D \dot{\sigma} + mg \xi^T \hat{e}_3. \tag{15}$$

The Euler–Lagrange equation from which the drone dynamics is developed is,

$$\frac{d}{dt}\left(\frac{\partial L}{\partial \dot{q}}\right) - \frac{\partial L}{\partial q} = \begin{bmatrix} F_\xi \\ \tau_\sigma \end{bmatrix}, \tag{16}$$

where the generalized coordinates are $q = [\xi^T \ \sigma^T]^T \in \mathrm{R}^9$. The term $F_\xi \in \mathrm{R}^3$ represents the nonconservative forces in the directions of the elements of ξ, while τ_σ are the moments acting on the angular coordinates in σ (these include three moments acting on the drone's body and three moments acting directly on seesaw angles). The Euler–Lagrange equation can be decoupled as,

$$\frac{d}{dt}\left(\frac{\partial L}{\partial \dot{\xi}}\right) - \frac{\partial L}{\partial \xi} = F_\xi \tag{17}$$

$$\frac{d}{dt}\left(\frac{\partial L}{\partial \dot{\sigma}}\right) - \frac{\partial L}{\partial \sigma} = \tau_\sigma \ . \tag{18}$$

Equation (17) represents the translational dynamics, and (18) represents the rotational dynamics. For the translation we get,

$$\begin{aligned} m\ddot{\xi} - mg\hat{e}_3 = F_\xi \quad \Rightarrow \quad \ddot{\xi} &= g\hat{e}_3 + \frac{1}{m} F_\xi \\ &= g\hat{e}_3 + \frac{1}{m} {}^e R_b F_b, \end{aligned} \tag{19}$$

where F_b is the total force generated by the propellers and expressed in body coordinates. For the generalized angular coordinates we obtain,

$$\begin{aligned} & D(\sigma)\ddot{\sigma} + \dot{D}(\sigma)\dot{\sigma} - \frac{1}{2}\frac{\partial}{\partial \sigma}\left(\dot{\sigma}^T D(\sigma)\dot{\sigma}\right) = \tau_\sigma \\ & \Rightarrow \\ & D(\sigma)\ddot{\sigma} = \left(\frac{1}{2}\frac{\partial}{\partial \sigma}\left(\dot{\sigma}^T D(\sigma)\right) - \dot{D}(\sigma)\right)\dot{\sigma} + \tau_\sigma \end{aligned} \tag{20}$$

and by defining $C(\sigma, \dot{\sigma}) = \frac{1}{2}\frac{\partial}{\partial \sigma}\left(\dot{\sigma}^T D(\sigma)\right) - \dot{D}(\sigma)$, it becomes,

$$\ddot{\sigma} = D^{-1}(\sigma)\left[\tau_\sigma + C(\sigma, \dot{\sigma})\dot{\sigma}\right] \ . \tag{21}$$

C. Actuation

We are now developing the expression of the nonconservative forces as a function of the propellers' angular velocity. The drone is actuated by six propellers divided into three couples, where each couple belongs to a seesaw. Each one of the six propellers generates a thrust (perpendicular to the propeller plane) and a pure torque; these are assumed to be proportional to the propeller angular speed according to,

$$f_{i,j} = k_f \omega_{i,j}^2 \ , \quad \tau_{i,j} = k_\tau \omega_{i,j}^2 \ . \tag{22}$$

In (22), $i \in \{\alpha, \beta, \gamma\}$ represents one of the three seesaws, and $j \in \{l, r\}$ represents the individual propeller on that seesaw (left-hand-side or right-hand-side) as described in Fig. 1. From a practical point of view $k_\tau \ll k_f$ (generally by two orders of magnitude), hence, a moment generated by a force couple (due to the difference in thrust forces) is much larger than the propellers' pure torque. Standard drones have no other means to generate the needed yaw moment other than this pure torque (this also includes standard hexacopters). As to the three-seesaw hexacopter, a much stronger yaw moment can be generated by tilting the seesaws. Hence, for the development of the drone's control laws, we neglect the influence of $\tau_{i,j}$ and based only on $f_{i,j}$. The thrust of each seesaw is,

$$\begin{aligned} f_\alpha &= (f_{\alpha,l} + f_{\alpha,r}) \\ f_\beta &= (f_{\beta,l} + f_{\beta,r}) \\ f_\gamma &= (f_{\gamma,l} + f_{\gamma,r}). \end{aligned} \tag{23}$$

These forces will be used to obtain the desired motion of the drone's body. Each thrust can be tilted; f_α by the angle α, f_β by β, and f_γ by γ. The seesaw's angular motion (α, β, γ) can be directly influenced by the moment generated by the thrust difference at each seesaw. Let d represent the distance between two propellers of a single seesaw, then,

$$\begin{aligned} \tau_\alpha &= d(f_{\alpha,l} - f_{\alpha,r}) \\ \tau_\beta &= d(f_{\beta,l} - f_{\beta,r}) \\ \tau_\gamma &= d(f_{\gamma,l} - f_{\gamma,r}). \end{aligned} \tag{24}$$

The total force acting on the drone is,

$$F_\xi = {}^e R_b F_b = {}^e R_b \left(F_{b,\alpha} + F_{b,\beta} + F_{b,\gamma}\right), \tag{25}$$

where F_b is the force vector represented by body coordinates. For the individual seesaws, we have,

$$\begin{aligned} & F_{b,\alpha} = {}^b R_\alpha F_\alpha = \begin{bmatrix} 0 \\ \mathrm{s}\alpha \\ -\mathrm{c}\alpha \end{bmatrix} f_\alpha, \ \ F_{b,\beta} = {}^b R_\beta F_\beta = \begin{bmatrix} \mathrm{s}\frac{\pi}{3}\mathrm{s}\beta \\ \mathrm{c}\frac{\pi}{3}\mathrm{s}\beta \\ -\mathrm{c}\beta \end{bmatrix} f_\beta \\ & F_{b,\gamma} = {}^b R_\gamma F_\gamma = \begin{bmatrix} -\mathrm{s}\frac{\pi}{3}\mathrm{s}\gamma \\ \mathrm{c}\frac{\pi}{3}\mathrm{s}\gamma \\ -\mathrm{c}\gamma \end{bmatrix}. \end{aligned} \tag{26}$$

Combining all of these forces together gives,

$$F_b = \begin{bmatrix} f_{b,x} \\ f_{b,y} \\ f_{b,z} \end{bmatrix} = \begin{bmatrix} (f_\beta \mathrm{s}\beta - f_\gamma \mathrm{s}\gamma)\mathrm{s}\frac{\pi}{3} \\ f_\alpha \mathrm{s}\alpha + (f_\beta \mathrm{s}\beta + f_\gamma \mathrm{s}\gamma)\mathrm{c}\frac{\pi}{3} \\ -f_\alpha \mathrm{c}\alpha - f_\beta \mathrm{c}\beta - f_\gamma \mathrm{c}\gamma \end{bmatrix}. \tag{27}$$

Assuming l is the distance from the seesaw center to the center of mass of the body, the three moments acting on the main body due to trust forces are,

$$\begin{aligned} \tau_\phi &= l\mathrm{s}\tfrac{\pi}{3}(-f_\beta \mathrm{c}\beta + f_\gamma \mathrm{c}\gamma) \\ \tau_\theta &= l f_\alpha \mathrm{c}\alpha - l\mathrm{c}\tfrac{\pi}{3}(f_\beta \mathrm{c}\beta + f_\gamma \mathrm{c}\gamma) \\ \tau_\psi &= l(f_\alpha \mathrm{s}\alpha - f_\beta \mathrm{s}\beta - f_\gamma \mathrm{s}\gamma). \end{aligned} \tag{28}$$

Lastly, in this subsection, the relation between the generated seesaws' total thrust and moment elements are represented

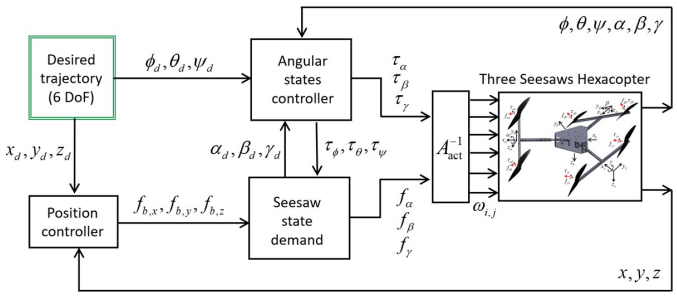

Fig. 3. Control system structure

compactly by,

$$\begin{bmatrix} f_\alpha \\ f_\beta \\ f_\gamma \\ \tau_\alpha \\ \tau_\beta \\ \tau_\gamma \end{bmatrix} = k_f \underbrace{\begin{bmatrix} 1 & 1 & 0 & 0 & 0 & 0 \\ 0 & 0 & 1 & 1 & 0 & 0 \\ 0 & 0 & 0 & 0 & 1 & 1 \\ d & -d & 0 & 0 & 0 & 0 \\ 0 & 0 & d & -d & 0 & 0 \\ 0 & 0 & 0 & 0 & d & -d \end{bmatrix}}_{A_{\text{act}}} \begin{bmatrix} \omega_{\alpha,l}^2 \\ \omega_{\alpha,r}^2 \\ \omega_{\beta,l}^2 \\ \omega_{\beta,r}^2 \\ \omega_{\gamma,l}^2 \\ \omega_{\gamma,r}^2 \end{bmatrix}, \quad (29)$$

where A_{act} is the actuation matrix that is clearly non-singular.

IV. Control

A. Control system structure

The control system structure is presented in Fig. 3. The control goal is to track a desired spatial trajectory represented by three position coordinates $x_d(t), y_d(t), z_d(t)$ and three angular coordinates $\phi_d(t), \theta_d(t), \psi_d(t)$. There are two main control laws working simultaneously, a position controller and an angular state controller. The position controller receives the desired position and generates the needed body forces (represented by $f_{b,x}, f_{b,y}, f_{b,z}$, in the body coordinate system). This control law uses the information (x, y, z) received from a position sensor (such as GPS). The required control force f_b is then fed to the Seesaw-state-demand block. The Seesaw-state-demand block (to be detailed in the following subsection) determines the required seesaw states, including the desired three seesaws' tilting angles $(\alpha_d, \beta_d, \gamma_d)$ and the required three seesaws' total forces $(f_\alpha, f_\beta, f_\gamma)$. The desired body angular state (represented by the desired Euler angles ϕ_d, θ_d, ψ_d) and the desired angular state of the seesaws $(\alpha_d, \beta_d, \gamma_d)$ form together the desired angular state σ_d (see (9)). The desired angular state is then compared to the measured angular states $(\phi, \theta, \psi$ by the drone's IMU and α, β, γ by onboard encoders) to generate six moments to be applied, three body moments $(\tau_\phi, \tau_\theta, \tau_\psi)$ and three seesaw moments $(\tau_\alpha, \tau_\beta, \tau_\gamma)$. The three-body moments are also fed to the Seesaw-state demand block. In the last stage, the demanded actuation is represented by six parameters, three seesaws' moments, and three seesaws' thrusts. This demand is translated to the individual rotating speed command $(\omega_{i,j})$ sent to each one of the six motors.

The Seesaw-state demand block is responsible for generating the required seesaw state. The calculation is based on (27) and (28), which can be unified into the following set of six coupled nonlinear equations (after replacing the actual seesaw angels α, β, γ with the demanded seesaw angles $\alpha_d, \beta_d, \gamma_d$),

$$\begin{aligned} f_{b,x} &= \mathrm{s}\tfrac{\pi}{3} f_\beta \mathrm{s}\beta_d - \mathrm{s}\tfrac{\pi}{3} f_\gamma \mathrm{s}\gamma_d \\ f_{b,y} &= f_\alpha \mathrm{s}\alpha_d + \mathrm{c}\tfrac{\pi}{3} f_\beta \mathrm{s}\beta_d + \mathrm{c}\tfrac{\pi}{3} f_\gamma \mathrm{s}\gamma_d \\ f_{b,z} &= -f_\alpha \mathrm{c}\alpha_d - f_\beta \mathrm{c}\beta_d - f_\gamma \mathrm{c}\gamma_d \\ \tau_\phi &= -l\mathrm{s}\tfrac{\pi}{3} f_\beta \mathrm{c}\beta_d + l\mathrm{s}\tfrac{\pi}{3} f_\gamma \mathrm{c}\gamma_d \\ \tau_\theta &= l f_\alpha \mathrm{c}\alpha_d - l\mathrm{c}\tfrac{\pi}{3} f_\beta \mathrm{c}\beta_d - l\mathrm{c}\tfrac{\pi}{3} f_\gamma \mathrm{c}\gamma_d \\ \tau_\psi &= l f_\alpha \mathrm{s}\alpha_d - l f_\beta \mathrm{s}\beta_d - l f_\gamma \mathrm{s}\gamma_d \end{aligned} \quad (30)$$

(to be solved for $\alpha_d, \beta_d, \gamma_d$, and $f_\alpha, f_\beta, f_\gamma$). The nonlinear set of equations can be represented as a linear set in the following way (where the unknowns are the force elements),

$$\begin{bmatrix} f_{b,x} \\ f_{b,y} \\ f_{b,z} \\ \tau_\phi \\ \tau_\theta \\ \tau_\psi \end{bmatrix} = \underbrace{\begin{bmatrix} 0 & 0 & \mathrm{s}\frac{\pi}{3} & 0 & -\mathrm{s}\frac{\pi}{3} & 0 \\ 1 & 0 & \mathrm{c}\frac{\pi}{3} & 0 & \mathrm{c}\frac{\pi}{3} & 0 \\ 0 & -1 & 0 & -1 & 0 & -1 \\ 0 & 0 & 0 & -l\mathrm{s}\frac{\pi}{3} & 0 & l\mathrm{s}\frac{\pi}{3} \\ 0 & l & 0 & -l\mathrm{c}\frac{\pi}{3} & 0 & -l\mathrm{c}\frac{\pi}{3} \\ l & 0 & -l & 0 & -l & 0 \end{bmatrix}}_{A_{\text{seesaw}}} \begin{bmatrix} f_\alpha \mathrm{s}\alpha_\mathrm{d} \\ f_\alpha \mathrm{c}\alpha_\mathrm{d} \\ f_\beta \mathrm{s}\beta_\mathrm{d} \\ f_\beta \mathrm{c}\beta_\mathrm{d} \\ f_\gamma \mathrm{s}\gamma_\mathrm{d} \\ f_\gamma \mathrm{c}\gamma_\mathrm{d} \end{bmatrix}. \quad (31)$$

As can be seen, the matrix A_{seesaw} is invertible, and it is always possible to find a solution for the seesaw-demanded states. This is the core reason why the six degrees of freedom of the main body can be controlled independently. Nevertheless, full actuation of the main body requires negligible seesaw dynamics (or sufficiently fast in practice). The solution of (31) is,

$$\begin{bmatrix} f_\alpha \mathrm{s}\alpha_\mathrm{d} \\ f_\alpha \mathrm{c}\alpha_\mathrm{d} \\ f_\beta \mathrm{s}\beta_\mathrm{d} \\ f_\beta \mathrm{c}\beta_\mathrm{d} \\ f_\gamma \mathrm{s}\gamma_\mathrm{d} \\ f_\gamma \mathrm{c}\gamma_\mathrm{d} \end{bmatrix} = \frac{2}{3l} \begin{bmatrix} l f_{b,y} + \mathrm{c}\frac{\pi}{3}\tau_\psi \\ -l\mathrm{c}\frac{\pi}{3} f_{b,z} + \tau_\theta \\ l\mathrm{s}\frac{\pi}{3} f_{b,x} + l\mathrm{c}\frac{\pi}{3} f_{b,y} - \mathrm{c}\frac{\pi}{3}\tau_\psi \\ -l\mathrm{c}\frac{\pi}{3} f_{b,z} - \mathrm{s}\frac{\pi}{3}\tau_\phi - \mathrm{c}\frac{\pi}{3}\tau_\theta \\ -l\mathrm{s}\frac{\pi}{3} f_{b,x} + l\mathrm{c}\frac{\pi}{3} f_{b,y} - \mathrm{c}\frac{\pi}{3}\tau_\psi \\ -l\mathrm{c}\frac{\pi}{3} f_{b,z} + \mathrm{s}\frac{\pi}{3}\tau_\phi - \mathrm{c}\frac{\pi}{3}\tau_\theta \end{bmatrix}. \quad (32)$$

From this result, we calculate,

$$\begin{aligned} f_\alpha &= \sqrt{(f_\alpha \mathrm{s}\alpha_d)^2 + (f_\alpha \mathrm{c}\alpha_d)^2} \\ f_\beta &= \sqrt{(f_\beta \mathrm{s}\beta_d)^2 + (f_\beta \mathrm{c}\beta_d)^2} \\ f_\gamma &= \sqrt{(f_\gamma \mathrm{s}\gamma_d)^2 + (f_\gamma \mathrm{c}\gamma_d)^2}, \end{aligned} \quad (33)$$

and,

$$\begin{aligned} \alpha_d &= \mathrm{atan2}(f_\alpha \mathrm{s}\alpha_d, f_\alpha \mathrm{c}\alpha_d) \\ \beta_d &= \mathrm{atan2}(f_\beta \mathrm{s}\beta_d, f_\beta \mathrm{c}\beta_d) \\ \gamma_d &= \mathrm{atan2}(f_\gamma \mathrm{s}\gamma_d, f_\gamma \mathrm{c}\gamma_d). \end{aligned} \quad (34)$$

B. Control law

There are two control laws supporting the control system described in Fig. 3. Both control laws use the same PD structure, which includes a feedback linearization element (due to the nonlinearity of the involved models), a feedforward

element (to allow the tracking demand) and a PD feedback for stability. The translational dynamical model is,

$$\ddot{\xi} = g\hat{e}_3 + \frac{1}{m}{}^{e}R_b F_b \,. \tag{35}$$

The position controller determines the value of F_b (with the three force elements $f_{b,x}, f_{b,y}, f_{b,z}$). It is chosen as,

$$F_b = {}^{b}R_e \left[m \left(\ddot{\xi}_d + k_{P\xi} e_\xi + k_{D\xi} \dot{e}_\xi - g\hat{e}_3 \right) \right], \tag{36}$$

where $e_\xi = \xi_d - \xi$ is the position tracking error (with $\xi_d = [x_d \;\; y_d \;\; z_d]^T$), and $k_{P\xi}, k_{D\xi}$ are diagonal matrices of control gains. The matrix ${}^{b}R_e = [{}^{r}R_b]^T$ is the inverse of ${}^{r}R_b$, and together with the gravity cancellation term $-ge_3$ they provide feedback linearization. The term $\ddot{\xi}_d$ serves as a feedforward element representing the expected change of the desired trajectory. Combining (35) and (36), the closed loop is,

$$\ddot{e}_\xi + k_{D\xi}\dot{e}_\xi + k_{P\xi} e_\xi = 0. \tag{37}$$

Now, the controller gains can be designed (e.g., by LQR) to maintain stability in (21). The angular state controller is developed from the same principles. The rotational dynamical model is,

$$\ddot{\sigma} = D^{-1}(\sigma)\left[\tau_\sigma + C(\sigma,\dot{\sigma})\dot{\sigma}\right]. \tag{38}$$

The angular state controller determines the value of τ_σ (with three body moments, $\tau_\phi, \tau_\theta, \tau_\psi$, and three seesaw moments $\tau_\alpha, \tau_\beta, \tau_\gamma$). It is chosen as,

$$\tau_\sigma = D(\sigma)\left[\ddot{\sigma}_d + k_{P\sigma} e_\sigma + k_{D\sigma}\dot{e}_\sigma\right] - C(\sigma,\dot{\sigma})\dot{\sigma}, \tag{39}$$

which results in a closed loop of the form,

$$\ddot{e}_\sigma + k_{D\sigma}\dot{e}_\sigma + k_{P\sigma} e_\sigma = 0, \tag{40}$$

where $e_\sigma = \sigma_d - \sigma$ is the angular tracking error (including the three desired Euler angles $(\phi_d, \theta_d, \psi_d)$ and the three desired seesaw angles $(\alpha_d, \beta_d, \gamma_d)$ from (34).

Remark. The closed-loop dynamics in (37) and (40) are ideal in the sense they assume equality of (α, β, γ) and $(\alpha_d, \beta_d, \gamma_d)$. This is due to the hierarchal nature of the control system structure, which simplifies the design. To support this assumption, the closed-loop dynamics of seesaw angles should be designed to be sufficiently faster than that of the body coordinates.

Remark. The three-seesaw hexacopter is not a fully actuated system, as (when including the state of the seesaws) it has nine degrees of freedom (and only six independent control inputs). Considering this fact, a hierarchical control system structure is an inevitable solution. Yet, it is significant that all six degrees of freedom of the drone's main body can be controlled independently, which highly expands the drone's applicability.

Remark. The focus of this study is on the dynamics and the control system structure of the three-seesaw hexacopter. Alternative and more advanced feedback laws, such as the integral backstepping from [16] or the interpolating controller from [6] (that copes with constraints), can replace the PD controller suggested here.

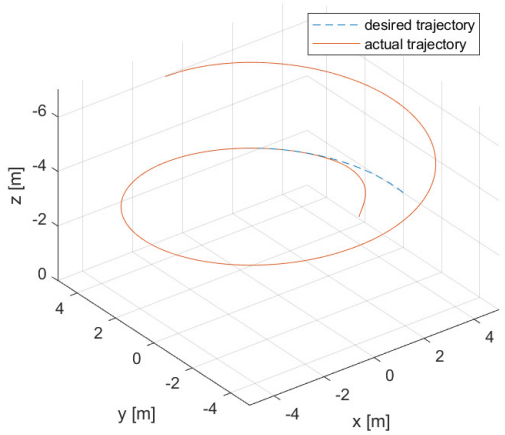

Fig. 4. Case 1 - Tracking a helical trajectory where the body of the drone is required to be level and the heading tangent to the required trajectory. The graph shows the convergence to the desired spatial trajectory.

C. Numerical example

We present two examples. In both the drone is required to track the same helical trajectory given by $x_d(t) = 5\cos(0.2t)[\mathrm{m}], y_d(t) = 5\sin(0.2t)[\mathrm{m}], z_d(t) = -2 - 0.1t[\mathrm{s}]$, but for a different desired angular state. In the first case, the drone is required to be level (i.e., $\phi_d = 0, \theta_d = 0$), while in the second case, it is commanded to tilt by $\frac{\pi}{8}[\mathrm{rad}]$ around its roll axis toward the helical center. For both cases, the heading direction (ψ_d) is controlled to be tangent to the planar (x_d, y_d) circle constructing the helix. The drone's physical parameters are: $m = 1[\mathrm{kg}]$, $d = 0.3[\mathrm{m}]$, $l = 0.3[\mathrm{m}]$, and I_b, $I_\alpha = I_\beta = I_\gamma$ are assumed to be diagonal. We neglect the influence of seesaw motion on the body's moment of inertia and use $I_{b,xx} = I_{b,yy} = 0.3\,[\mathrm{kg\,m^2}]$, $I_{b,zz} = 0.06\,[\mathrm{kg\,m^2}]$ for the simulation. Additionally, for all seesaws, $I_{xx} = I_{zz} = 0.002\,[\mathrm{kg\,m^2}]$ and $I_{yy} = 0.0001\,[\mathrm{kg\,m^2}]$. The initial conditions are, $\xi(0) = [4,\, 1,\, -1]^T\,[\mathrm{m}]$, and $\sigma(0) = 0$, and all initial velocities are zero. All controller gains were designed by LQR with respect to a double integrator model. The seesaw gains were designed for the quickest response with weighting coefficients of 500 (for the tracking errors) and 50 (for tracking error derivatives). The gains responsible for the translational motion were designed to be the slowest, with weighting coefficients of 10 and 5, and for the orientation of the body, the weighting coefficients are 50 and 10. To break the algebraic loop formed by the Angular state controller and the Seesaw state demand blocks (in Fig. 3), the demanded seesaw angles are filtered by a low-pass filter of the form $100/(s + 100)$. The obtained drone's trajectory of case 1 is presented in Fig. 4, while the six angular states are depicted in Fig. 5, and the thrust generated by each propeller is illustrated in Fig. 6. The result shows convergence to the desired spatial trajectory while keeping the body's angular state close to zero. The angular motion of the seesaws enables the tilted thrust forces required for the spatial motion. The simulation results of case

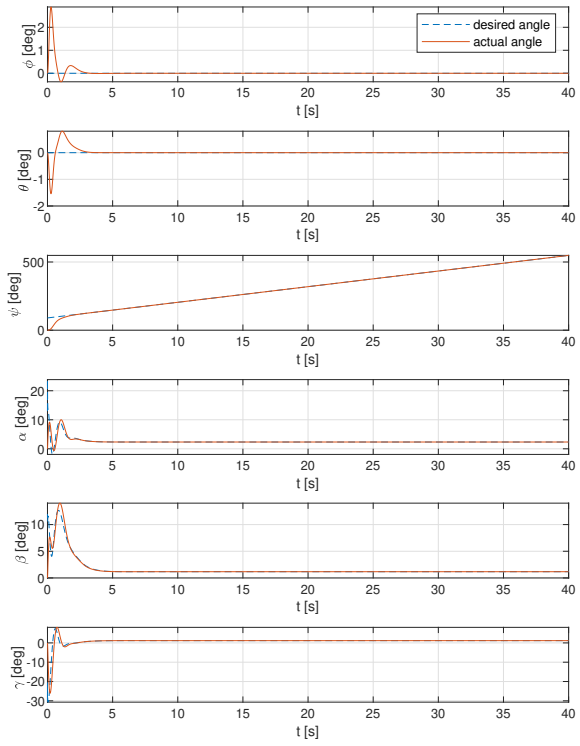

Fig. 5. Case 1 - Tracking a helical trajectory where the body of the drone is required to be level and the heading tangent to the required trajectory. The graph shows the tracking performance of all angular state variables.

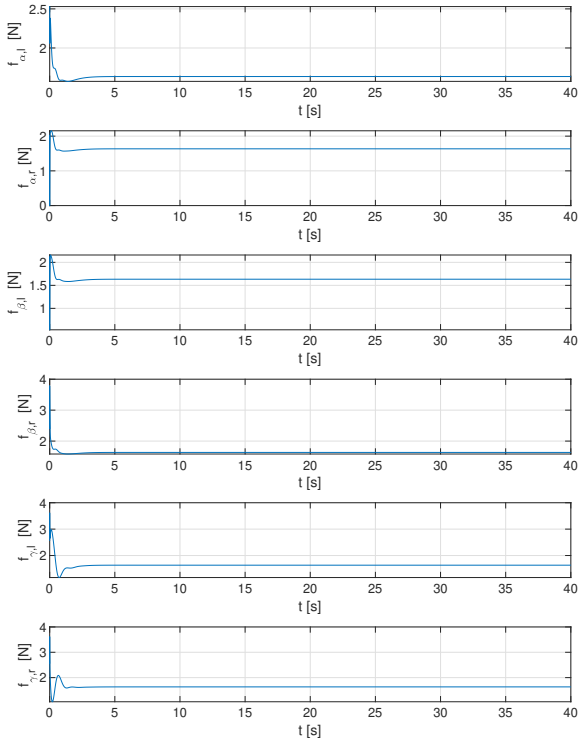

Fig. 6. Case 1 - Tracking a helical trajectory where the body of the drone is required to be level and the heading tangent to the required trajectory. The graph shows the thrust generated by each propeller.

2 are presented in Fig. 7, Fig. 8 and Fig. 9. The key point to observe is the similar spatial motion (as in case 1) but with a different controlled angular orientation of the drone's body. This unique feature of the three-seesaw hexacopter arises from its mechanical structure, which is based on freely rotating seesaws.

V. Conclusion

In this study, we suggested an unconventional hexacopter drone. The drone utilizes a unique structure of three seesaws allowing directing the total body thrust in any required direction, independently from the body's angular state. This allows independent control of all six body degrees of freedom with just six propellers and with no additional actuators. To control the complex structure, we suggested a control system based on three main elements: a position controller, an angular state controller, and a Seesaw-state demands module. The ability of the drone to track a desired spatial trajectory, independent of its (main body) angular state, has been demonstrated numerically. Our future work will examine the practical challenges involved in propelling drones by seesaws.

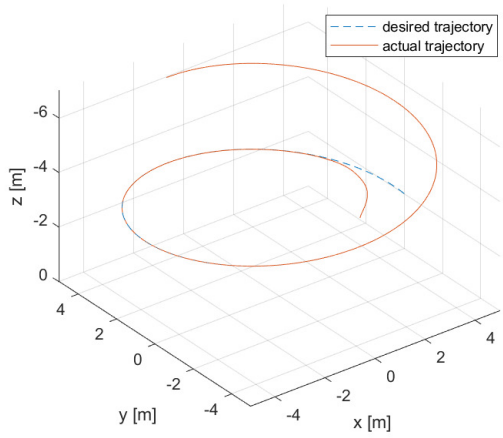

Fig. 7. Case 2 - Tracking a helical trajectory where the body of the drone is required to be tilted by $\pi/8$ rad toward the helical center. The graph shows the convergence to the desired spatial trajectory.

References

[1] M. Schuster, D. Bernstein, P. Reck, S. Hamaza, and M. Beitelschmidt, "Automated Aerial Screwing with a Fully Actuated Aerial Manipu-

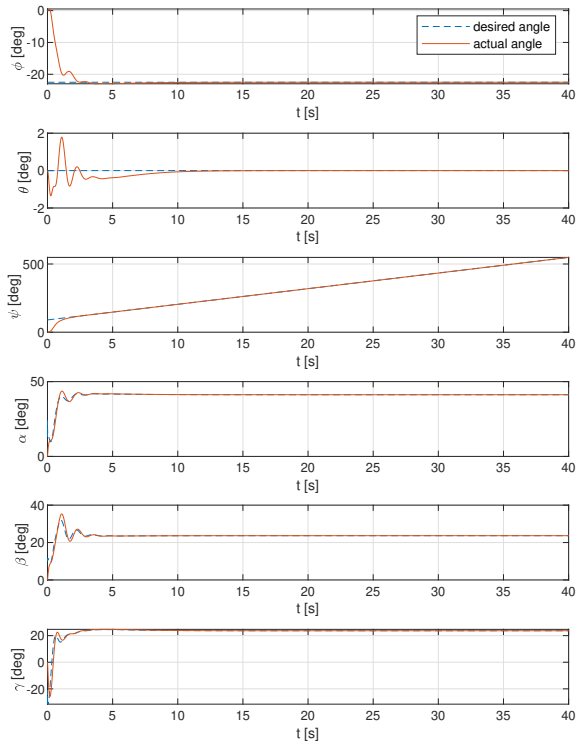

Fig. 8. Case 2 - Tracking a helical trajectory where the body of the drone is required to be tilted by $\pi/8$ rad toward the helical center. The graph shows the tracking performance of all angular state variables.

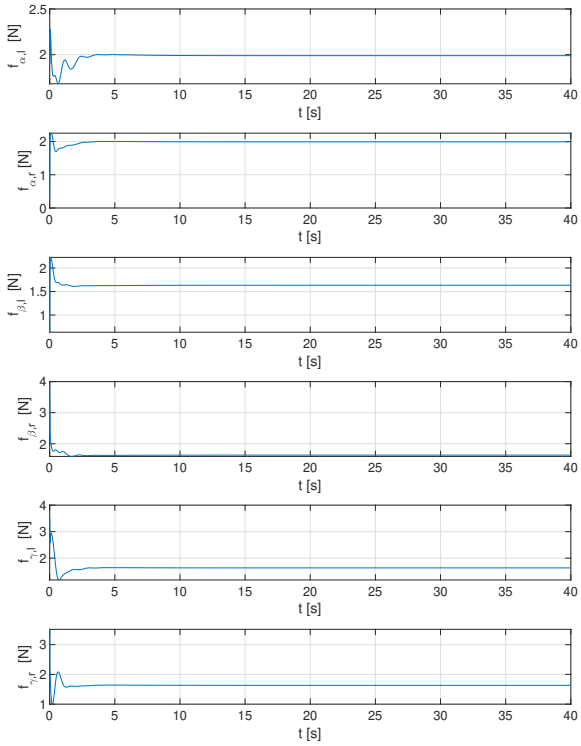

Fig. 9. Case 2 - Tracking a helical trajectory where the body of the drone is required to be tilted by $\pi/8$ rad toward the helical center. The graph shows the thrust generated by each propeller.

lator," IEEE/RSJ International Conference on Intelligent Robots and Systems (IROS), 2022.

[2] R. Jiao, J. Li, Y. Rong, and T. Hou, "Nonlinear Model Predictive Impedance Control of a Fully Actuated Hexarotor for Physical Interaction," Sensors 2023, 23, 5231. https://doi.org/10.3390/s23115231.

[3] C. Yao, J. Krieglstein, and K. Janschek, "Modeling and Sliding Mode Control of a Fully-actuated Multirotor with Tilted Propellers," IFAC PapersOnLine 51-22 (2018) 115–120.

[4] P. Zheng , X. Tan, B. Bahadir Kocer , E. Yang, and M. Kovac, "TiltDrone: A Fully-Actuated Tilting Quadrotor Platform," IEEE Robotics and Automation Letters, Vol. 5, No. 4, October 2020.

[5] M. Odelga, P. Stegagno, and H. H. Bülthoff, "A Fully Actuated Quadrotor UAV with a Propeller Tilting Mechanism: Modeling and Control," IEEE International Conference on Advanced Intelligent Mechatronics (AIM) Banff, Alberta, Canada, July 12–15, 2016.

[6] E. Kaballo, S. Arogeti, "Simple Interpolating Control with Non-Symmetric Input Constraints for a Tilt-Rotor UAV", to be presented in 2023 International Conference on Unmanned Aircraft Systems (ICUAS), Chania, Crete, June 2024.

[7] G. Flores and A. Flores, "Robust Nonlinear Control for the Fully Actuated Hexa-Rotor: Theory and Experiments," IEEE Control Systems Letters, Vol. 7, 2023.

[8] M. Schuster, D. Bernstein, C. Yao, K. Janscheck, M. Beitelschmidt, "Comparison of design approaches of fully actuated aerial robots based on maximum wrench generation and minimum energy consumption," IFAC PapersOnLine 52-15 (2019) 603–608

[9] G. Jiang, R. M. Voyles, J. J. Choi, "Precision Fully-Actuated UAV for Visual and Physical Inspection of Structures for Nuclear Decommissioning and Search and Rescue," IEEE International Symposium on Safety, Security, and Rescue Robotics (SSRR), 2018.

[10] J. Y. S. Lee, K. K. Leang, W. Yim, "Design and Control of a Fully-Actuated Hexrotor for Aerial Manipulation Applications," J. Mechanisms Robotics. Aug 2018, 10(4): 041007, https://doi.org/10.1115/1.4039854.

[11] D. Kotarski, P. Piljek, J. Kasa´c, and D. Majeti´c, "Performance Analysis of Fully Actuated Multirotor Unmanned Aerial Vehicle Configurations with Passively Tilted Rotors," Appl. Sci. 2021, 11, 8786. https://doi.org/10.3390/app11188786.

[12] P. Shu, F. Li, J. Zhao, M. Oya, "Robust Adaptive Control for A Novel Fully-Actuated Octocopter UAV with Wind Disturbance," Journal of Intelligent and Robotic Systems (2021) 103: 6 https://doi.org/10.1007/s10846-021-01450-x.

[13] C. Probine, D. Yang, K. A. Stol, and N. Kay, "Model Predictive Control on a Fully-actuated Octocopter for Wind Disturbance Rejection", 14th Annual International Micro Air Vehicle Conference And Competition, September 11-15, 2023, Aachen, Germany.

[14] C. Shi, K. Wang, and Y. Yu, "Expandable Fully Actuated Aerial Vehicle Assembly: Geometric Control Adapted from an Existing Flight Controller and Real-World Prototype Implementation," Drones 2022, 6, 272. https://doi.org/10.3390/drones6100272.

[15] D. Yecheskel, and S. Arogeti, " Modeling and Control of a Hexacopter with a Rotating Seesaw" 14th International Conference on Control, Automation, Robotics and Vision, Phuket, 2016.

[16] D. Yecheskel, S. Arogeti, "A Fully-Actuated Drone with Rotating Seesaws", in the Proceedings of 2023 International Conference on Unmanned Aircraft Systems (ICUAS), Warsaw, June 2023.

[17] D. Kastelan, M. Konz, J. Rudolph, "Fully Actuated Tricopter with Pilot-Supporting Control," IFAC-PapersOnLine 48-9 (2015) 079–084.

[18] D. K. Nguyen, V. V. Putov, and V. N. Sheludko, "Adaptive Robust Control of a Tricopter with Rotary Propellers under Uncertainty and Limited Input Actions," IEEE International Conference on Control in Technical Systems (CTS) 2023, DOI: 10.1109/CTS59431.2023.10289028.